Mechanical Stresses in a Linear Plastic FGM Hollow and Solid Rotational Disk

M. Jabbari, A. Hatefkia, M. Shokouhfar[*]

South Tehran Branch, Islamic Azad University, Tehran, Iran

ABSTRACT

In this paper, an analytical solution for computing the plastic & linear plastic stresses and critical angular velocity in a FGM hollow & solid rotating disk is developed. It has been assumed that the modulus of elasticity and yield strength were varying through thickness of the FGM material according to a power law relationship. The Poisson's ratio were considered constant throughout the thickness. In the analysis presented here the effect of non-homogeneity in FGM rotating disk was implemented by choosing a dimensionless parameter, named m, which could be assigned an arbitrary value affecting the stresses in the rotating disk. Distribution of stresses in radial and circumferential directions for FGM rotating disk under the influence of angular velocity were obtained. Graphs of variations of stress, critical angular velocity versus radius of the rotating disk were plotted. The direct method is used to solve the Navier equations.

© 2013 IAU, Arak Branch.All rights reserved.

Keywords: Hollow & solid disk; Non-homogenous; Axisymmetric; FGM; Elastic-plastic analysis

1 INTRODUCTION

FUNCTIONALLY graded material is heterogeneous material in which the elastic and thermal properties change from one surface to the other, gradually and continuously. Since ceramic has good resistance to heat, corrosion, and erosion and metal has high fracture toughness, ceramic-metal FGM may work at super high-temperatures or under high temperature differences and also corrosive fields. In effect, the governing equations of temperature and stress distributions are coordinate dependent as the material properties are functions of position.

There are a number of analytical thermal and stress calculations for functionally graded material in the one-dimensional case for thick cylinders and spheres [1,2]. The authors have considered non-homogeneous material properties as linear function of radius. Jabbari et al. [3] presented a general solution for mechanical and thermal stresses in a functionally graded hollow cylinder due to non-axisymmetric steady-state load. They applied separation of variables and complex Fourier series to solve the heat conduction and Navier equations. Poultangari et al. [4] presented a solution for the functionally graded hollow spheres under non-axisymmetric thermo-mechanical loads. Lu yunbing et al. [5] analyzed the steady state temperature distribution and the associated thermal stress distribution of a 3-layer composite cylinder system with material ingredient changing continuously in the middle FGM layer and a set of formulas for the temperature and the thermal stresses are obtained. Shariyat et al. [6] presented the nonlinear transient thermal stress and elastic wave propagation of thick temperature-dependent FGM cylinders, using a second-order point-collocation method. In another work [7], he found an algorithm for nonlinear transient behavior analysis of thick functionally graded cylindrical vessels or pipes with temperature-dependent material properties

---

[*] Corresponding author.
E-mail address: miladshokouhfar@gmail.com (M. Shokouhfar).

under thermo-mechanical load. Chen and Lim [8] presented elastic mechanical behavior of nano-scaled FGM films incorporating surface energies. Afsar and Sekine [9] presented inverse problems of material distributions for prescribed apparent fracture toughness in FGM coatings around a circular hole in infinite elastic media. Tajeddini et al. [10] discussed the three-dimensional free vibration of thick circular and annular isotropic and functionally graded (FG) plates with variable thickness along the radial direction. Nosier and Fallah [11], based on the first-order shear deformation plate theory with the von Karman non-linearity, presented the non-linear axisymmetric and asymmetric behavior of functionally graded circular plates under transverse mechanical loading. Zhang and Zhou [12] conducted a theoretical analysis of FGM thin plates based on the physical neutral surface. Fazelzadeh and Hosseini [13] discussed the aero-thermoelastic behavior of supersonic rotating thin-walled beams made of functionally graded materials. Ootao and Tanigawa [14] analyzed the transient thermo elastic problem of functionally graded thick strip due to non-uniform heat supply. They obtained the exact solution for the two-dimensional temperature change in a transient state, and thermal stresses of a simply supported strip under the state of plane strain condition. Jabbari et al. [15] studied the mechanical and thermal stresses in functionally graded hollow cylinder due to radial symmetric loads. They assumed the temperature distribution to be a function of radial direction. They applied a direct method to solve the heat conduction and Navier equations. Farid et al. [16] presented three-dimensional temperature dependent free vibration analysis of functionally graded material curved panels resting on two-parameter elastic foundation using a hybrid semi-analytic differential quadrature method. Bagri and Eslami [17] analyzed the generalized coupled thermoelasticity of functionally graded annular disk considering the Lord–Shulman theory. Jabbari et al [18] studied an axisymmetric mechanical and thermal stresses in a thick short length functionally graded material cylinder. They applied separation of variables and complex Fourier series to solve the heat conduction and Navier equation. Zamani-nejad and Rahimi [19], using the infinitesimal theory of elasticity, derived closed-form solutions for the one-dimensional steady-state thermal stresses in a rotating functionally graded (FGM) pressurized thick-walled hollow circular cylinder under generalized plane strain and plane stress assumptions, respectively. Batra and Iaccarino [20] found closed-form solutions for axisymmetric plane strain deformations of a functionally graded circular cylinder comprised of an isotropic and incompressible second-order elastic material with elastic module varying only in the radial direction. Cylinder's inner and outer surfaces are loaded by hydrostatic pressures. Three-dimensional thermo-elastic analysis of a functionally graded cylindrical panel with finite length and subjected to non uniform mechanical and steady-state thermal loads are carried out by Shao and Wang [21].

There are limited papers on the subject of plasticity of FGM structures. Shabana and Noda [22] presented thermo-elasto-plastic stresses in functionally graded materials subjected to thermal loading taking residual stresses of the fabrication process into consideration. Eraslan and Akis [23] presented plane strain analytical solutions for a functionally graded elastic–plastic pressurized tube. Eraslan and Arslan [24] discussed the plasticity of plane strain rotating graded hollow shafts. The elasto-plastic response of a long functionally graded tube subjected to internal pressure is given by Eraslan and Akis [25]. Alla et al. [26] analyzed the elastic–plastic problem of 2D-FGM plates made of ZrO2, 6061-T6 and Ti-6Al-4V under transient thermal loading. Lu [27] presented a stress analysis for the functionally graded disc under mechanical loads and a steady state temperature distribution. Jahromi [28] obtained the elasto-plastic stresses in a functionally graded rotating disk. Sadeghian and Toussi [29] presented the elasto-plastic axisymmetric thermal stress analysis of functionally graded cylindrical vessel.

The classical method of analysis with linear strain hardening curve is to combine the equilibrium equations with the stress-strain and strain-displacement relations to arrive at the governing equation in terms of the stress components. The stress equations are solved in elastic and plastic regions for the solid and hollow FGM rotational disk, analytically. The analysis is presented for two types of applicable boundary conditions. In this work, an analytical method is presented for mechanical stress analysis of an FGM hollow disk based on the linear plasticity. It is assumed that the modulus of elasticity vary through the thickness of FGM material according to a power law relationship. The Poisson ratio is considered constant throughout the thickness. The stress equation is solved analytically by a direct method.

2   EQUATIONS
2.1 Linear plastic stresses

The linear plastic stress-strain relations for plane-strain conditions are:

$$\epsilon_{rr} = \frac{1}{E}(\sigma_{rr} - \upsilon\sigma_{\theta\theta}) + \epsilon_{rr}^{p}, \qquad \epsilon_{rr,r} + \left(\frac{\epsilon_{\theta\theta} - \epsilon_{rr}}{r}\right) = 0, \qquad \epsilon_{rr}^{p} + \epsilon_{\theta\theta}^{p} = 0, \qquad \epsilon_{rr,r} + \left(\frac{\epsilon_{\theta\theta} - \epsilon_{rr}}{r}\right) = 0,$$

$$\epsilon_{rr} = u_{,r}, \qquad \epsilon_{\theta\theta} = \frac{u}{r}$$

(1)

where (,r) denotes differentiation with respect to *r*. where σ_{ij} and ε_{ij} (i, j = r, θ) are the stress and strain tensors, and λ and μ are Lame´ coefficients related to the modulus of elasticity *E* and Poisson's ratio υ as:

$$\lambda = \frac{\upsilon E}{(1+\upsilon)(1-2\upsilon)} \qquad \mu = \frac{E}{2(1+\upsilon)}$$

(2)

The equilibrium equation in the radial direction, disregarding the body force and the inertia term, is:

$$\sigma_{rr,r} + \left(\frac{\sigma_{rr} - \sigma_{\theta\theta}}{r}\right) = -\rho r\omega^2 \qquad \sigma_{\theta\theta} = r\sigma_{rr,r} + \sigma_{rr} + \rho r^2\omega^2$$

(3)

To obtain the equation of stresses in terms of plastic strain for the FGM rotating disk the functional relationship of the material properties must be known. Since the disk's material is assumed to be graded along the r direction, the modulus of elasticity, the density and yield strength are assumed to be described with a power law as:

$$E = E_0\left(\frac{R}{l}\right)^{m_1} = E_0 r^{m_1} \qquad \rho = \rho_0\left(\frac{R}{l}\right)^{m_2} = \rho r^{m_2} \qquad \sigma_0 = \sigma_0(\frac{R}{l})^{m_4} = \sigma_0 r^{m_4}$$

(4)

where E_0 and ρ_0 and σ_0 are the material constants and m_1 and m_2 and m_4 are the power law indices of the material. We may further assume that Poisson's ratio is constant.
Using relations (1)-(4), the equation in term of the stresses is:

$$\sigma_{rr,rr} + g_1\frac{1}{r}\sigma_{rr,r} + g_2\frac{1}{r^2}\sigma_{rr} = g_3\omega^2 r^{m_2} + g_4 r^{m_1-1}\epsilon_{rr,r}^{p} + g_5 r^{m_1-2}\epsilon_{rr}^{p}$$

(5)

The constants of g_1, g_2, g_3, g_4 and g_5 are presented at Appendix A
Eq. (5) is the differential equation with general and particular solutions. The general solution is assumed to have the form

$$\sigma_n^g(r) = Kr^x$$

(6)

Substituting Eq. (6) into Eq. (5) yields

$$x^2 + x(g_1 - 1) + g_2 = 0$$

(7)

Eq. (7) has two real roots x_1 and x_2 :

$$x_1 = \frac{-(g_1-1)}{2} + (\frac{(g_1-1)^2}{4} - g_2)^{0.5} \qquad x_2 = (\frac{-(g_1-1)}{2} - (\frac{(g_1-1)^2}{4} - g_2)^{0.5}$$

(8)

Thus the general solution is:

$$\sigma^g(r) = K_1 r^{x_1} + K_2 r^{x_2}$$

(9)

The particular solution $\sigma^g(r)$ is assumed to be of the form

$$\sigma^p(r) = L_1 r^{m_1+1} + L_2 r^{m_1} + L_3 r^{2+m_2} \tag{10}$$

Substituting Eq. (10) into Eq. (5) equating the coefficients of the identical powers that they are presented at Appendix A.

The complete solution for σ_{rr} is the sum of the general and particular solutions as:

$$\sigma_{rr} = K_1 r^{x_1} + K_2 r^{x_2} + L_1 \epsilon_{rr,r}^p r^{m_1+1} + L_2 \epsilon_{rr}^p r^{m_1} + L_3 r^{2+m_2} \omega^2 \tag{11}$$

$$\sigma_{\theta\theta} = (x_1 K_1 + K_1) r^{x_1} + (x_2 K_2 + K_2) r^{x_2} + L_1 \epsilon_{rr,rr}^p r^{m_1+2} + [(m_1+1) L_1 \epsilon_{rr,r}^p + L_2 \epsilon_{rr,r}^p + L_1 \epsilon_{rr,r}^p] r^{m_1+1}$$
$$+ (m_1 L_2 \epsilon_{rr}^p + L_2 \epsilon_{rr}^p) + (3+m_2) L_3 r^{2+m_2} \omega^2 + \rho_0 r^{2+m_2} \omega^2 \tag{12}$$

To determine the constants K_1 and K_2, consider the boundary conditions for hollow disk's stresses given by

$$\sigma_{rr}(a) = 0 \qquad \sigma_{rr}(b) = 0 \tag{13}$$

Substituting the boundary conditions (13) into Eq. (12), the constants of integration for stresses yield and they are presented at Appendix A.

The elastic stresses are [27]

$$\sigma_{rr} = \frac{E_0}{1-v^2} [(z_1 + \upsilon) H_1 r^{m_1+z_1-1} + (z_2 + \upsilon) H_2 r^{m_1+z_2-1} + (-m_1 + 3 + \upsilon + m_2) D\omega^2 r^{2+m_2}]$$

$$\sigma_{\theta\theta} = \frac{E_0}{1-v^2} [(\upsilon z_1 + 1) H_1 r^{m_1+z_1-1} + (\upsilon z_2 + 1) H_2 r^{m_1+z_2-1} + (-\upsilon m_1 + 3v + 1 + \upsilon m_2)] \tag{14}$$

The coefficients of Eq. (14) are presented at Appendix A.

In terms of graph of (ϵ_{rr}^p, s) we obtain the gradient (M*E) of graph then we obtain the equation of linear plastic strain for thermal stresses as [30]

$$\epsilon_{rr}^p = \frac{1-M}{M}(1-s) \qquad s = s_{rr} - s_{\theta\theta} \qquad s_{rr} = \frac{\sigma_{rr}}{\sigma_0 r^{m_4}} \qquad s_{\theta\theta} = \frac{\sigma_{\theta\theta}}{\sigma_0 r^{m_4}} \tag{15}$$

By substituting Eq. (14) into Eq. (15) the ϵ_{rr}^p yields as:

$$\epsilon_{rr}^p = \frac{1-M}{M}(1 - \frac{E_0}{(1-\upsilon)\sigma_0}(\upsilon z_1 + 1 - z_1 - \upsilon) H_1 r^{m_1-m_4+z_1-1} (\upsilon z_2 + 1 - z_2 - \upsilon) H_2 r^{m_1-m_4+z_2-1} + (-\upsilon m_1 + 2\upsilon -$$
$$2 + vm_2 + m_1 - m_2) D\omega^2 r^{2+m_2-m_4}]) \tag{16}$$

From Eq. (15) we obtain the $\epsilon_{rr,r}^p$ as:

$$\epsilon_{rr,r}^p = \frac{M-1}{M}(s_{,r}) \tag{17}$$

2.2 Perfect plastic

Tresca's criterion is as [30]

$$\left| \sigma_{\theta\theta} - \sigma_{rr} \right| = \sigma_0 r^{m_4} \tag{18}$$

By substituting the Eq. (3) into Eq. (18) we obtain

$$\sigma_{rr,r} = -\rho r \omega^2 + \frac{\sigma_0 r^{m_4}}{r} \tag{19}$$

By solving the Eq.(19) ,the σ_{rr} yields as:

$$\sigma_{rr}^{p} = \frac{-\rho_0 r^{m_2+2}\omega^2}{2+m_2} + \frac{1}{m_4}\sigma_0 r^{m_4} + c \tag{20}$$

By substituting the Eq. (20) into Eq.(18), the $\sigma_{\theta\theta}$ yields as:

$$\sigma_{\theta\theta}^{p} = \frac{-\rho_0 r^{m_2+2}\omega^2}{2+m_2} + \frac{1}{m_4}\sigma_0 r^{m_4} + \sigma_0 r^{m_4} + c \tag{21}$$

By substituting the Eq. (20) into Eq. (13), the constant c yields and it is presented at Appendix A. The boundary conditions for solid disk are as:

$$\sigma_{rr}(a) = \text{finite} \qquad\qquad \sigma_{rr}(b) = 0 \tag{22}$$

By substituting the Eq. (20) into Eq. (22) ,the constant c yields and it is presented at Appendix B. Using relations (1)–(4), the Navier equation in terms of the displacement is:

$$u_{,r} + \frac{u}{r} = \frac{2 d_1 \rho_0 \omega^2 r^{2-m_1+m_2}}{2+m_2} + d_1\left(\frac{2}{m_4}+1\right)\sigma_0 r^{m_4-m_1} + d_1(\frac{2\rho_0 a^{2+m_2}\omega^2}{2+m_2} - \frac{2}{m_4}\sigma_0 a^{(m_4)})r^{(-m_1)} \tag{23}$$

The coefficient of d_1 is presented at Appendix A.

Eq. (23) is the differential equation with general and particular solutions. The general solution is assumed to have the form

$$u_n^g(r) = B r^{\eta} \tag{24}$$

Substituting Eq. (24) into Eq. (23) yields

$$\eta B r^{\eta-1} + B r^{\eta-1} = 0 \tag{25}$$

Eq. (25) has real root η as:

$$\eta = -1 \tag{26}$$

Thus, the general solution is:

$$u_n^g(r) = \frac{B}{r} \tag{27}$$

The particular solution $u_n^p(r)$ is assumed to be of the form

$$u_n^p(r) = I_1 r^{3-m_1+m_2} + I_2 r^{m_4-m_1+1} + I_3 r^{-m_1+1}$$ (28)

By substituting Eq. (28) into Eq. (23), the coefficients of the identical powers yields and they are presented at Appendix A.

Complete solution for *u(r)* is the sum of the general and particular solutions as:

$$U = \frac{B}{r} + I_1 r^{3-m_1+m_2} + I_2 r^{m_4-m_1+1} + I_3 r^{-m_1+1}$$ (29)

Substituting Eq. (29) into Eqs. (1), the strains are obtained as:

$$\epsilon_{rr} = \frac{-B}{r^2} + (3-m_1+m_2)I_1 r^{2-m_1+m_2} + (m_4-m_1+1)I_2 r^{m_4-m_1} + (-m_1+1)I_3 r^{-m_1}$$

$$\epsilon_{\theta\theta} = \frac{B}{r^2} + I_1 r^{2-m_1+m_2} + I_2 r^{m_4-m_1} + I_3 r^{-m_1}$$ (30)

Then by substituting the Eq.(30) into Eq. (1) the plastic strains yield as:

$$\epsilon_{rr}^p = \frac{-B}{r^2} + (3-m_1+m_2)I_1 r^{2-m_1+m_2} + (m_4-m_1+1)I_2 r^{m_4-m_1} + (-m_1+1)I_3 r^{-m_1} - \frac{1}{E}(\sigma_{rr} - \upsilon\sigma_{\theta\theta})$$

$$\epsilon_{\theta\theta}^p = \frac{B}{r^2} + I_1 r^{2-m_1+m_2} + I_2 r^{m_4-m_1} + I_3 r^{-m_1} - \frac{1}{E}(\sigma_{\theta\theta} - \upsilon\sigma_{rr})$$ (31)

By substituting Eq. (1) , Eq. (30) and Eq. (31) into Eq. (24), the coefficient of B yields and it is presented at Appendix A.

2.3 Critical angular velocity

The critical angular velocity is a velocity that causes the stresses go beyond the elastic region and come to plastic criteria. So this is one of the more important factors in designing.

By substituting Eq. (14) into the Eq. (18), the critical angular velocity yields as:

$$\omega = \left(\frac{(1-\upsilon^2)\sigma_0 r^{m_4}}{E_0\left[(1-z_1)(1-\upsilon)H_3 r^{m_1+z_1-1} + (1-z_2)(1-\upsilon)H_4 r^{m_1+z_2-1} + (-\upsilon m_1 + 2\upsilon + m_1 - 2 - m_2 + \upsilon m_2)Dr^{2+m_2}\right]}\right)^{0.5}$$ (32)

The coefficients of H_3 and H_4 are presented at Appendix A.

3   RESULTS AND DISCUSSION

As an example 1, consider a hollow disk of inner radius $a = 0.1\,\text{m}$, and outer radius $b = 1\,\text{m}$, Poisson's ratio is taken to be 0.3, and the modulus of elasticity at the inner radius are $E_i = 200\,\text{Gpa}$ and the density $\rho_0 = 7850\,\text{Kg}/\text{m}^3$. For simplicity of analysis, the power law coefficients for ρ, E and σ_0 are considered to be the same, i.e. $m_2 = m_1 = m_4 = m$. The boundary conditions for the hollow disk are assumed as $\sigma_{rr}(a) = 0\,\text{Mpa}$, and $\sigma_{rr}(b) = 0\,\text{Mpa}$ and the angular velocity is $\omega = 150\,\text{rad}/\text{s}$. As an example 2, consider a hollow disk of inner radius $a = 0.1m$, and outer radius $b = 1m$, Poisson's ratio is taken to be 0.3, and the modulus of elasticity at the inner radius are $E_i = 79\,\text{Gpa}$ and the density $\rho_0 = 2700\,\text{Kg}/\text{m}^3$. For simplicity of analysis, the power law coefficients for

ρ, E and σ_0 are considered to be the same, i.e. $m_2 = m_1 = m_4 = m$. The boundary conditions for the hollow disk are assumed as $\sigma_{rr}(a) = 0$ Mpa, and $\sigma_{rr}(b) = 0$ Mpa and the angular velocity is $\omega = 490 \frac{\text{rad}}{\text{s}}$ [19]. Variations of the radial stress $\hat{\sigma}_r = \dfrac{\sigma_r}{\rho_0 \omega^2 b^2}$ and circumferential stress $\hat{\sigma}_\theta = \dfrac{\sigma_\theta}{\rho_0 \omega^2 b^2}$ and radial displacement $\hat{u} = \dfrac{uE_0}{\rho_0 \omega^2 b^3}$ are given as normalized. As an example 3, consider a thin disk on outer radius $= 1m$, and the angular velocity is $\omega = 200 \frac{\text{rad}}{\text{s}}$ and the other parameters are the same as previous example.

Fig. 1 shows the radial elastic stress by substituting $\epsilon_{rr}^p = \epsilon_{rr,r}^p = 0$ in linear plastic stress (Example 1). Effect of power-law index on the radial elastic stress is shown in this figure. By increasing grading parameter m, the normalized radial stresses at the inner section rise in a disc. The radial stress is observed to be compressive in the inner region of the disk and tensile over the outer region. Fig. 2 shows the circumferential elastic stress by substituting $\epsilon_{rr}^p = \epsilon_{rr,r}^p = 0$ in linear plastic stress (Example 1). Effect of power-law index on the circumferential elastic stress is shown in this figure. By increasing grading parameter m, the normalized circumferential stresses at the inner section rise in a disc. The absolute maximum tangential stresses occur at the inner edge. Fig. 3 shows the effective elastic stress by substituting $\epsilon_{rr}^p = \epsilon_{rr,r}^p = 0$ in linear plastic stress (Example 1). Effect of power-law index on the effective elastic stress is shown in this figure. The magnitude of the tangential stress is higher than that of the radial Stress. Fig. 4 shows the radial distribution of radial displacement (Example 1). Effect of power-law index on the radial displacement is shown in this figure. Fig. 5 shows the critical angular velocity (Example 1). Effect of power-law index on the critical angular velocity is shown in this figure. The absolute maximum angular velocity occurs at the inner edge. Fig. 6 shows the normalized elasticity modulus through the radius of hollow disc for different values of the power low index m (Example 1). Fig. 7 shows the radial distribution of radial plastic stress for positive power low coefficients. Effect of power-law index on the radial plastic stress is shown in this figure. By increasing grading parameter m, the radial plastic stresses at the outer section rise in a disc. Fig. 8 shows the radial distribution of radial plastic stress for negative power low coefficients (Example 1). Effect of power-law index on the radial plastic stress is shown in this figure. Fig. 9 shows the radial distribution of circumferential plastic stress for positive power low coefficients (Example 1). Effect of power-law index on the 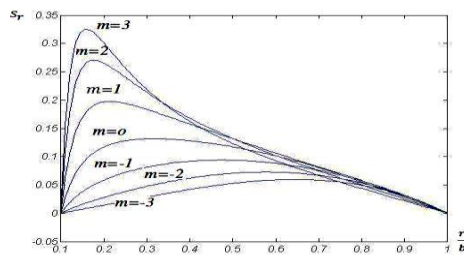circumferential plastic stress is shown in this figure. Fig. 10 shows the radial distribution of circumferential plastic stress for negative power low coefficients (Example 1). Effect of power-law index on the circumferential plastic stress is shown in this figure.

Fig. 1
Radial elastic stress by substituting $\epsilon_{rr}^p = \epsilon_{rr,r}^p = 0 =$ in linear plastic stress. (Example 1)
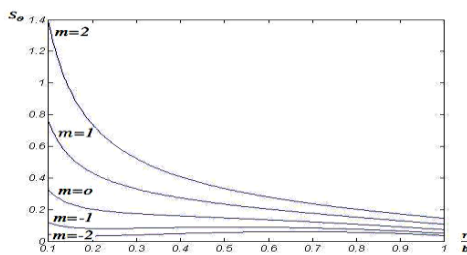

Fig. 2
Circumferential elastic stress by substituting $\epsilon_{rr}^p = \epsilon_{rr,r}^p = 0$ in linear plastic stress .(Example 1)
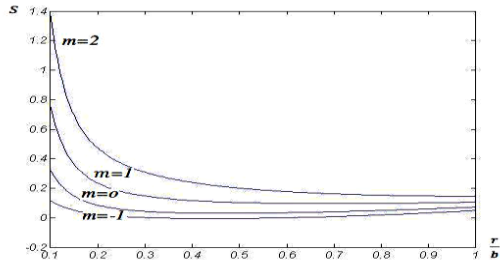
Fig. 3
Effective elastic stress by substituting $\epsilon_{rr}^{p} = \epsilon_{rr,r}^{p} = 0$ in linear plastic stress. (Example 1)
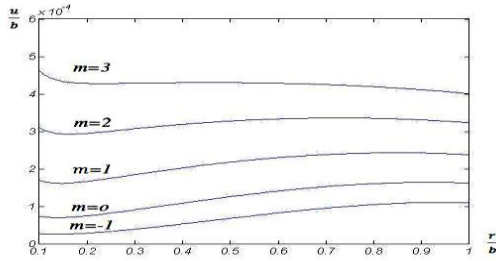

Fig. 4
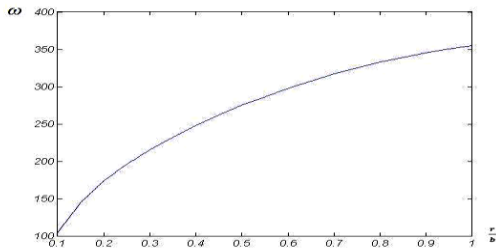Radial distribution of radial displacement.(Example 1)

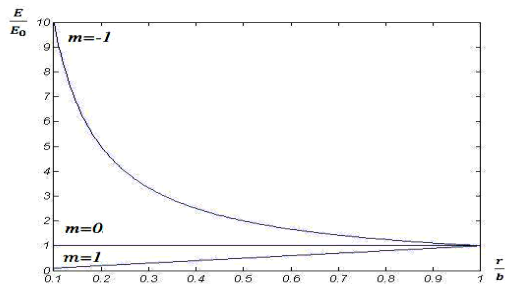**Fig. 5**
Critical angular velocity.(Example 1)

Fig. 6
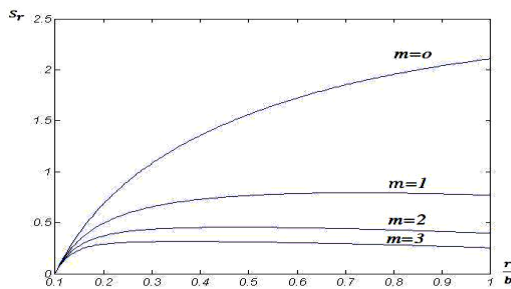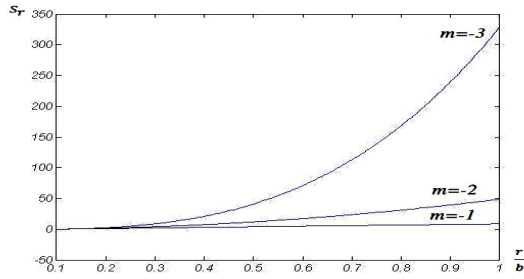Normalized elasticity modulus through the radius of hollow disc for different values of the power low index *m*.(Example1)

Fig. 7
Radial distribution of radial plastic stress for positive power low coefficients.(Example 1)

Fig. 8
Radial distribution of radial plastic stress for negative power low coefficients. (Example 1)
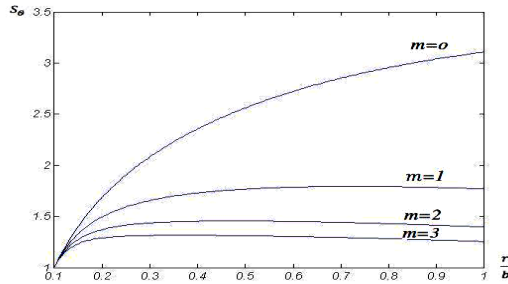
Fig. 9
Radial distribution of circumferential plastic stress for positive power low coefficients. (Example 1)
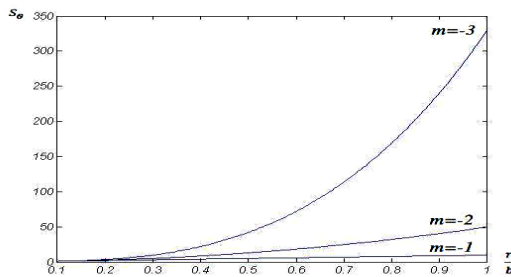
Fig. 10
Radial distribution of circumferential plastic stress for negative power low coefficients. (Example 1)

Fig. 11 shows the comparing of radial elastic stress [27] (shows with square) with radial linear plastic stress by substituting $\epsilon_{rr}^{p} = \epsilon_{rr,r}^{p} = 0$ in stress formula that they should be the same (Example 2). By increasing grading parameter m, the normalized radial stresses at the inner section rise in a disc Fig. 12 shows the comparing of circumferential elastic stress[27] (shows with square) with circumferential linear plastic stress by substituting $\epsilon_{rr}^{p} = \epsilon_{rr,r}^{p} = 0$ in stress formula that they should be the same (Example 2). Fig. 13 indicates the comparing of radial displacement [27] (shows with square) with radial linear plastic displacement by substituting $\epsilon_{rr}^{p} = \epsilon_{rr,r}^{p} = 0$ in stress formula that they should be the same (Example 2). The maximum measure of displacmeent occurs at outer edge of disk. Fig. 14 shows the radial distribution of radial plastic displacement (Example 1). Effect of power-law index on the radial plastic displacement is shown in this figure. The maximum measure of displacmeent occurs at outer edge of disk. It is observed that the radial plastic displacement component is maximum at the outer surface of the disk and its magnitude gradually decreases towards the inner surface of the disk. Fig. 15 indicates the radial distribution of radial plastic strain for positive power low coefficients (Example 1). Fig. 16 indicates the radial distribution of radial plastic strain for negative power low coefficients (Example 1). Fig. 17 indicates the radial distribution of circumferential plastic strain for positive power low coefficients (Example 1).Fig. 18 indicates the radial distribution of circumferential plastic strain for negative power low coefficients (Example 1). Fig.19 shows the radial distribution of radial stress of linear plastic when $m = 1$ for different values of slope of linear strain hardening curve M (Example 1). The minimum measure of radial linear stress occurs at $M = 0$ that is plastic region (Example 1).
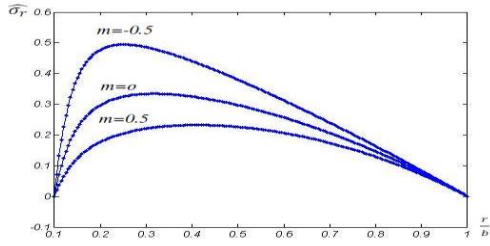
Fig.11
Comparing of radial elastic stress[27](shows with square) with radial linear plastic stress by substituting in stress formula that they should be the same.(Example 2)
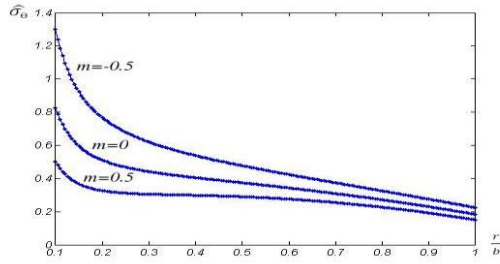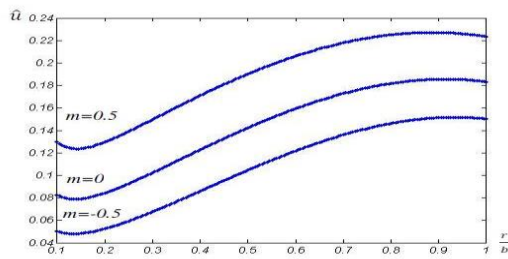

Fig.12
Comparing of circumferential elastic stress [27] (shows with square) with circumferential linear plastic stress by substituting $\epsilon_{rr}^{p} = \epsilon_{rr,r}^{p} = 0$ in stress formula that they should be the same. (Example 2)

Fig.13
Comparing of radial elastic displacement [27] (shows with square) with radial linear plastic displacement by substituting $\epsilon_{rr}^{p} = \epsilon_{rr,r}^{p} = 0$ in stress formula that they should be the same.(Example 2)
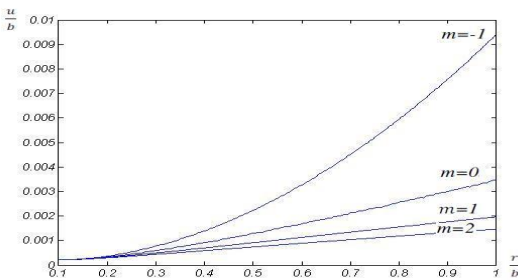

Fig.14
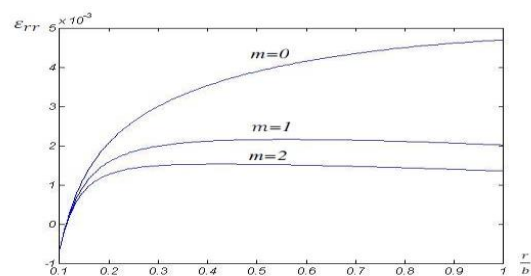Radial distribution of radial plastic displacement.(Example1)

Fig.15
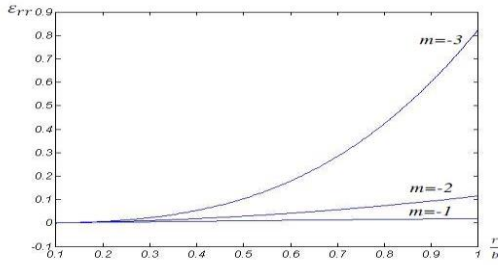Radial distribution of radial plastic strain for positive power low coefficients. (Example 1)

Fig.16
Radial distribution of radial plastic strain for negative power low coefficients. (Example 1)
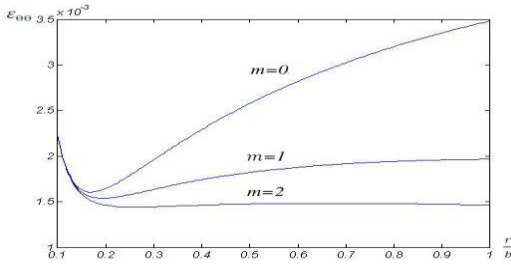

Fig.17
Radial distribution of circumferential plastic strain for positive power low coefficients. (Example 1)
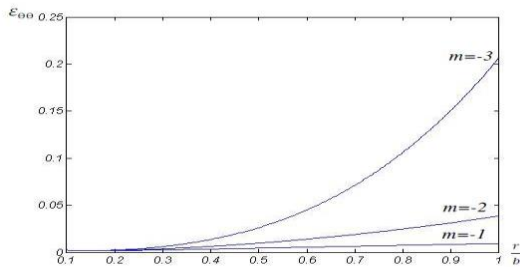

Fig.18
Radial distribution of circumferential plastic strain for negative power low coefficients.(Example 1)
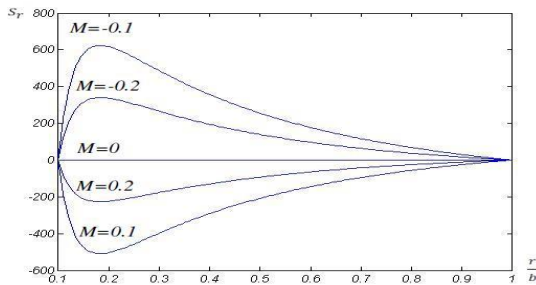

Fig.19
Radial distribution of radial stress of linear plastic for $m = 1$. (Example 1)

The radial stress is observed to be compressive in the inner region of the disk and tensile over the outer region. Fig.20 shows the radial distribution of circumferential stress of linear plastic when $m = 1$ for different values of slope of linear strain hardening curve M. The minimum measure of circumferential linear stress occurs at $M = 0$ that is plastic region (Example 1). Fig. 21 shows the radial distribution of effective stress of linear plastic when $m = 1$ for different values of slope of linear strain hardening curve M. The magnitude of the tangential stress is higher than that of the radial Stress (Example 1). Fig. 22 shows the radial distribution of radial stress of linear plastic when $m = -1$ for different values of slope of linear strain hardening curve M (Example 1). Fig. 23 shows the radial distribution of circumferential stress of linear plastic when $m = -1$ for different values of slope of linear strain hardening curve M (Example 1). Fig. 24 indicates the radial distribution of effective stress of linear plastic when $m = -1$ for different values of slope of linear strain hardening curve M (Example 1). Fig. 25 shows the comparing of

radial plastic stress [28] (shows with square) with radial linear plastic stress by substituting $M = 0$ in stress formula that it should give the plastic stress formula. The thing that justify the difference of two graphs is that the yield strength, density and modulus of elasticity are different in these two articles (Example 3). Fig.26 shows the comparing of circumferential plastic stress [28] (shows with square) with circumferential linear plastic stress by substituting $M = 0$ in stress formula that it should give the plastic stress formula. The maximum measure of radial plastic stress ocurs at iner edg. The thing that justify the difference of two graphs is that the yield strength, density and modulus of elasticity are different in these two articles (Example 3). Fig. 27 shows the relative density versus the angular velocities developing incipient and plasticity in a FGM disk. The maximum measure of circumferential plastic stress ocurs at iner edg. (Example 1)
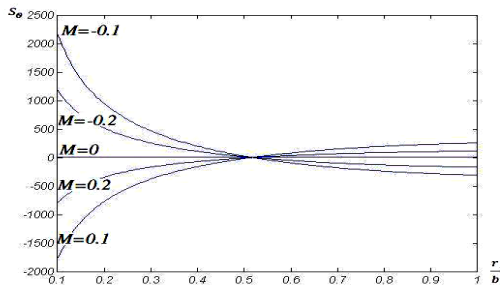

Fig. 20
Radial distribution of circumferential stress of linear plastic for $m = 1$. (Example 1)
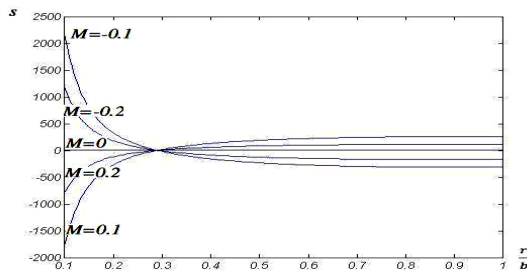

Fig. 21
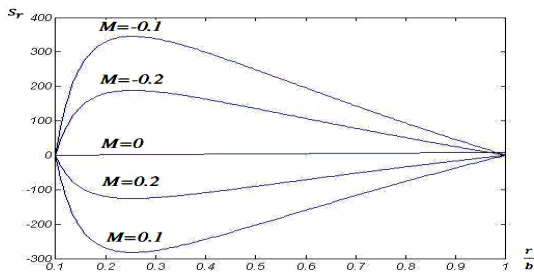Radial distribution of effective stress of linear plastic for $m = 1$. (Example 1)

Fig. 22
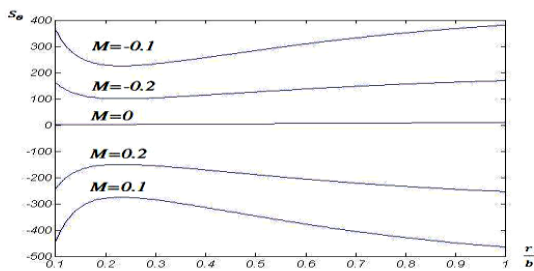Radial distribution of radial stress of linear plastic for $m = -1$. (Example 1)

Fig. 23
Radial distribution of circumferential stress of linear plastic for $m = -1$. (Example 1)
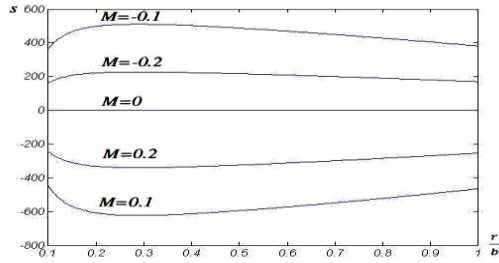
Fig. 24
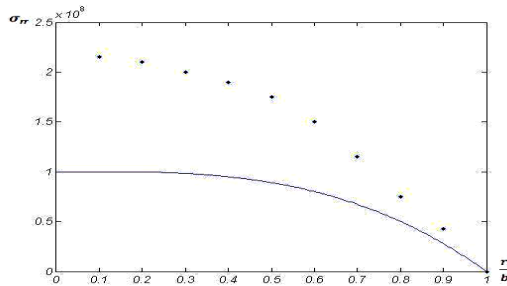Radial distribution of effective stress of linear plastic for $m = -1$. (Example 1)

Fig. 25
Comparing of redial plastic stress [28](shows with square) with radial linear plastic stress by substituting $M = 0$ in stress formula that it should give the plastic stress formula. (Example 3)
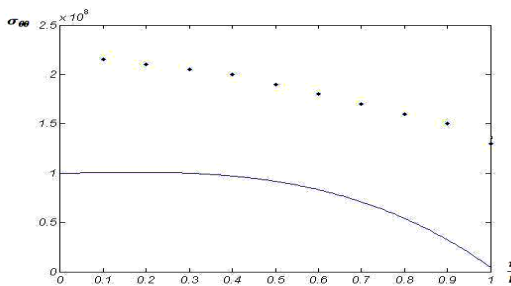

Fig .26
Comparing of circumferential plastic stress [28] (shows with square) with circumferential linear plastic stress by substituting $M = 0$ in stress formula that it should give the plastic stress formula. (Example 3)
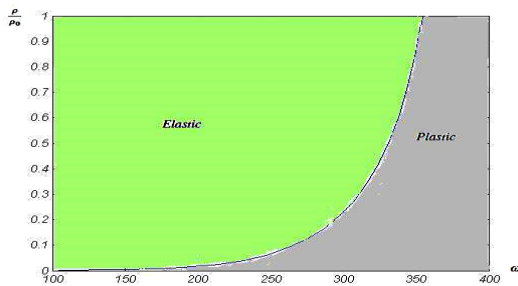
Fig. 27
Relative density versus the angular velocities developing incipient and plasticity in a FGM disk. (Example 1)

4   CONCLUSIONS

In the present work, an attempt has been made to study the problem of general solution for the stresses in a plastic & linear plastic FGM hollow & solid disk. The method of solution is based on the direct method and uses power series, rather than the potential function method. The advantage of this method is its mathematical power to handle mathematical function for the plastic & linear plastic stresses boundary conditions. The material properties and yield strength through the graded direction are assumed to be nonlinear with a power law distribution. Depending on applied boundary condition, by selecting optimum value of *m*, desirable level of radial and circumferential stresses

could be obtained in FGM cylinders with respect to those in homogenous ones. By setting $m=0$ in every equations, radial and circumferential stresses expressions turned to homogenous ones which could approve the validity of formulations. By setting $M=0$ in linear plastic equations, radial and circumferential stresses expressions turned to plastic stress which could approve the validity of formulations. We can find the critical angular velocity that are very important for designing. By increasing grading parameter m, the normalized radial stresses at the inner section rise in a disc. The absolute maximum tangential stresses occur at the inner edge. The normalized radial and tangential stresses and radial displacements in a disc due to centrifugal force increase with increasing m. The normalized tangential stress components at the inner edge are found to be higher than those at the outer edge. The normalized radial displacements at the outer surface are higher than those at the inner surface and by increasing m. The magnitude of the tangential stress is higher than that of the radial Stress. The measure of linear stress decreases close the plastic region. It is observed that the radial plastic displacement component is maximum at the outer surface of the disk and its magnitude gradually decreases towards the inner surface of the disk. The radial stress is observed to be compressive in the inner region of the disk and tensile over the outer region.

APPENDIX A

$$g_1 = (3 - m_1) \qquad g_2 = m_1(\upsilon - 1) \qquad g_3 = \rho_0(m_1 - 3 - v - m_2) \qquad g_4 = E_0 \qquad g_5 = 2E_0$$

$$L_1 = \frac{g_4}{(m_1 + 1)m_1 + (m_1 + 1)g_1 + g_2} \qquad L_2 = \frac{g_5}{m_1 g_1 + g_2 + (m_1 - 1)m_1} \qquad L_3 = \frac{g_3}{\left[(m_2^2 + 3m_2 + 2) + (2 + m_2)g_1 + g_2\right]}$$

$$K_2 = \frac{L_1\left(\epsilon_{b,r}^p a^{x_1} b^{m_1+1} - \epsilon_{a,r}^p b^{x_1} a^{m_1+1}\right) + L_2\left(\epsilon_b^p a^{x_1} b^{m_1} - \epsilon_a^p b^{x_1} a^{m_1}\right) + L_3\omega^2\left(a^{x_1} b^{2+m_2} - b^{x_1} a^{2+m_2}\right)}{a^{x_2} b^{x_1} - a^{x_1} b^{x_2}}$$

$$K_1 = \frac{L_1\left(\epsilon_{b,r}^p a^{x_2} b^{m_1+1} - \epsilon_{a,r}^p b^{x_2} a^{m_1+1}\right) + L_2\left(\epsilon_b^p a^{x_2} b^{m_1} - \epsilon_a^p b^{x_2} a^{m_1}\right) + L_3\omega^2\left(a^{x_2} b^{2+m_2} - b^{x_2} a^{2+m_2}\right)}{a^{x_1} b^{x_2} - a^{x_2} b^{x_1}}$$

$$D = \frac{-(1 - v^2)\rho_0}{E_0[(-m_1 + m_2 + 3)(-m_1 + m_2 + 2) + (m_1 + 1)(-m_1 + m_2 + 3) + (vm_1 - 1)]}$$

$$d_2 = (z_1 + \upsilon) \qquad d_3 = (z_2 + \upsilon) \qquad d_4 = D(-m_1 + 3 + \upsilon + m_2)$$

$$H_2 = \frac{d_4\omega^2\left[b^{2+m_2} a^{m_1+z_1-1} - a^{2+m_2} b^{m_1+z_1-1}\right]}{d_3\left[b^{m_1+z_1-1} a^{m_1+z_2-1} - b^{m_1+z_2-1} a^{m_1+z_1-1}\right]} \qquad H_1 = \frac{d_4\omega^2\left[b^{2+m_2} a^{m_1+z_2-1} - a^{2+m_2} b^{m_1+z_2-1}\right]}{d_3\left[b^{m_1+z_2-1} a^{m_1+z_1-1} - b^{m_1+z_1-1} a^{m_1+z_2-1}\right]}$$

$$c = \frac{\rho_0 a^{2+m_2}\omega^2}{2 + m_2} - \frac{1}{m_4}\sigma_0 a^{m_4} \qquad d_1 = \frac{(1 - \upsilon)}{E_0}$$

$$I_1 = \frac{-2d_1\rho_0\omega^2}{(m_2 + 2)(4 - m_1 + m_2)} \qquad I_2 = \frac{d_1\left(\dfrac{2}{m_4} + 1\right)\sigma_0}{m_4 - m_1 + 2} \qquad I_3 = \frac{d_1\left(\dfrac{2\rho_0 a^{2+m_2}\omega^2}{2 + m_2} - \dfrac{2}{m_4}\sigma_0 a^{m_4}\right)}{2 - m_1}$$

$$B = \frac{a^2\left[(6 - 2m_1 + 2v + 2m_2)I_1 r^{2-m_1+m_2} + (2m_4 - 2m_1 + 2 + 2\upsilon)I_2 r^{m_4-m_1} + (-2m_1 + 2 + 2\upsilon)I_3 r^{-m_1}\right]}{(2 - 2\upsilon)}$$

$$H_3 = \frac{H_1}{\omega^2} \qquad H_4 = \frac{H_2}{\omega^2}$$

$$\text{(A.1)}$$

APPENDIX B

$$c = \frac{\rho_0 b^{2+m_2} \omega^2}{2+m_2} - \frac{1}{m_4} \sigma_0 b^{m_4} \qquad (B.1)$$

REFERENCES

[1]   Lutz M.P., Zimmerman R.W., 1996, Thermal stresses and effective thermal expansion coefficient of functionally graded Sphere, *Journal of Thermal Stresses* **19**:39-54.

[2]   Zimmerman R.W., Lutz M.p., 1999, Thermal stresses and thermal expansion in a uniformly heated functionally graded cylinder, *Journal of Thermal Stresses* **22**:177-188.

[3]   Jabbari M., Sohrabpour S., Eslami MR., 2003, Generalsolution for mechanical and thermal stresses in functionally graded hollow cylinder due to radially symmetric loads. *Journal of Applied Mechanics* **70**:111-119.

[4]   Poultangari R., Jabbari M., Eslami M.R., 2008, Functionally graded hollow spheres under non-axisymmetric thermo-mechanical loads, *International Journal of Pressure Vessels and Piping* **85**: 295-305.

[5]   Yunbing L., Kayin Z., Jinsheng X., Dongsheng W., 1999, Thermal stresses analysis of ceramic/metal functionally gradient material cylinder, Applied Mathematics and Mechanics **20**(4):413-417.

[6]   Shariyat M., Lavasani S.M.H., Khaghani M., 2010, Nonlinear transient thermal stress and elastic wave propagation analyses of thick temperature-dependent FGM cylinders, using a second-order point-collocation method, *Applied Mathematical Modelling* **34**(4):898-918.

[7]   Shariyat M., 2009,A nonlinear hermitian transfinite element method for transient behavior analysis of hollow functionally graded cylinders with temperature-dependent materials under thermo-mechanical loads, *International Journal of Pressure Vessels and Piping* **86**: 280-289.

[8]   Lü C.F., Chen W.Q., Lim C.W., 2009, Elastic mechanical behavior of nano-scaled FGM films incorporating surface energies, *Composites Science and Technology* **69**:1124-1130.

[9]   Afsar A.M., Sekine H., 2002, Inverse problems of material distributions for prescribed apparent fracture toughness in FGM coatings around acircular hole in infinite elastic media, *Composites Science and Technology* **62**:1063-1077.

[10]   Tajeddini V., Ohadi A., Sadighi M., 2011, Three-dimensional free vibration of variable thickness thick circular and annular isotropic and functionally graded plates on Pasternak foundation, *International Journal of Mechanical Sciences* **53**: 300-308.

[11]   Nosier A., Fallah F., 2009, Non-linear analysis of functionally graded circular plates under asymmetric transverse loading, *International Journal of Non-Linear Mechanics* **44**:928- 942.

[12]   Da-Guang Z., You-He Z., 2008, A theoretical analysis of FGM thin plates based on physical neutral surface, *Computational Materials Science* **44**:716-720.

[13]   Fazelzadeh S.A., Hosseini M., 2007, Aerothermoelastic behavior of supersonic rotating thin-walled beams made of functionally graded materials, *Journal of Fluids and Structures* **23**:1251-1264.

[14]   Ootao Y., Tanigawa Y., 2004, Transient thermoelastic problem of functionally graded thick strip due to non uniform heat supply, *Composite Structures* **63**(2):139-146.

[15]   Jabbari M., Sohrabpour S., Eslami M.R., 2002, Mechanical and thermal stresses in a functionally graded hollow cylinder due to radially symmetric loads , *International Journal of Pressure Vessels and Piping* **79**: 493-497.

[16]   Farid M., Zahedinejad P., Malekzadeh P., 2010, Three-dimensional temperature dependent free vibration analysis of functionally graded material curved panels resting on two-parameter elastic foundation using a hybrid semi-analytic, differential quadrature method, *Materials and Design* **31**: 2-13.

[17]   Bagri A., Eslami M.R., 2008, Generalized coupled thermoelasticity of functionally graded annular disk considering the Lord–Shulman theory, *Composite Structures* **83**: 168-179.

[18]   Jabbari M., Bahtui A., Eslami M.R., 2009, Axisymmetric mechanical and thermal stresses in thick short length functionally graded material cylinder, *International Journal of Pressure Vessels and Piping* **86**:296-306.

[19]   Zamani Nejad M., Rahimi G. H., 2009, Deformations and stresses in rotating FGM pressurized thick hollow cylinder under thermal load, *Scientific Research and Essay* **4**(3):131-140.

[20]   Batra R.C., Iaccarino G.L., 2008, Exact solutions for radial deformations of a functionally graded isotropic and incompressible second-order elastic cylinder, *International Journal of Non-Linear Mechanics* **43**:383-398.

[21]   Shao Z.S., Wang T.J., 2006, Three-dimensional solutions for the stress fields infunctionally graded cylindrical panel with finite lengthand subjected to thermal/mechanical loads, *International Journal of Solids and Structures* **43**:3856-3874.

[22]   Shabana Y.M., Noda N.,2001, Thermo-elasto-plastic stresses in functionally graded materials subjected to thermal loading taking residual stresses of the fabrication process into consideration , *Composites: Part B* **32**:111-121.

[23]   Eraslan A.N., Akis T., 2006, Plane strain analytical solutions for a functionally graded elastic–plastic pressurized tube, *International Journal of Pressure Vessels and Piping* **83**: 635-644.

[24]   Eraslan A.N., Eraslan E., 2007, Plane strain analytical solutions to rotating partially plastic graded hollow shafts, *Turkish Journal of Engineering and Environmental Sciences* **31**: 273-288.

[25]   Eraslan A.N.*,* Akis T., 2005, Elastoplastic response of a long functionally graded tube subjected to internal pressure, *Turkish Journal of Engineering and Environmental Sciences* **29**:361-368.

[26]   Alla M. N., Ahmed K. I. E., Allah I. H. 2009, Elastic–plastic analysis of two-dimensional functionally graded materials under thermal loading, *International Journal of Solids and Structures* **46**:2774-2786.

[27]   Lu H.Ç.,2011, Stress analysis in a functionally graded disc under mechanical loads and a steady state temperature distribution, *Indian Academy of Sciences Sadhana* **36** (1): 53-64.

[28]   Jahromi B. H., 2012, Elasto-plastic stresses in a functionally graded rotating disk, *Journal of Engineering Materials and Technology* **134**: 021004-11.

[29]   Sadeghian M.,Toussi H. E., 2012, Elasto-plastic axisymmetric thermal stress analysis of functionally graded cylindrical vessel , *Journal of Basic and Applied Scientific Research* **2**(10):10246-10257.

[30]   Mendelson A., 1986, Plasticity: Theory and Application, New York, Mac Millan.